Development of an Electro Impedance Tomography-based Platform for Measurement of burial Depth of Cables in Subsea Sediments

Andreas Schuldei*, Tim Suthau*, Fabian John*, Gunther Ardelt* and Horst Hellbrück*
* Luebeck University of Applied Sciences, Germany
Department of Electrical Engineering and Computer Science, Center of Excellence CoSA
Email: {andreas.schuldei, tim.suthau, fabian.john, gunther.ardelt, horst.hellbrueck}@th-luebeck.de

***Abstract*—Cables buried in the seabed are objects of interests especially as companies have to verify that the buried depth of the cables is in the expected range, typically $1\ m$. Although several measurement systems have been designed in the past, there is no solution available that provides an accuracy of $\pm 10\ cm$ for this purpose. In our approach we suggest to model and measure the electrical field and electrical impedance to determine the depth of a sea cable. In the first step we develop an electrical static field model for analytic investigations. We validate the model by a simulation tool and provide results for critical environmental parameters that affect our measurement accuracy.**

***Index Terms*—submarine cables, underwater detection, seabed objects, measurement systems**

I. Introduction and Related Work

The detection of objects and materials in the seabed is becoming increasingly important with regard to activities of the offshore industry. Because power transmission cables can be damaged or destroyed by other users of the oceans and by environmental impacts, protective measures must be taken. The most common protection is the laying of cables within the seabed. Installation depths of 1 to 3 meters have been customary. Due to special requirements or natural sediment shifting, the sediment cover can grow to more than 5 meters. In order to check the effectiveness of the protective measures, and to guarantee the integrity of the submarine installations, regular tests of the cable routes are necessary. Specifically, the depth and the thickness of the sediment cover of a cable must be verified.

Systems based on passive induction sensing e.g. manufactured by Tinsley [1] are known to vary in accuracy. Additionally, measurements are hard to reproduce, especially since they depend on the operator's subjective assessment. Active pulse induction methods as in [2] depend on calibration, since water properties like pressure, temperature and salinity influence the method and they have a limited range.

Szyrowski [3] concludes his in-depth investigation into the topic with the statement that existing developments show a significant need for simple, intelligent remote sensing systems for buried sub-sea cables, especially at a greater range.

In [4] and [5] initial attempts to detect objects with Electro Impedance Tomography (EIT) in subsea sediment were made. No information has been given regarding the vertical measurements' accuracy.

Xu et. al. [6] analyzes the current development of underwater cable shape detection methods, including visual, acoustic, magnetic detection, and multisensor fusion detection, and describes the advantages and disadvantages.

To the best of our knowledge, there is no cable surveying system on the market that reaches a depth of 5m with an accuracy of $\pm 10\,\mathrm{cm}$ on power transmission cables in the high-voltage range. All currently available methods and systems are subject to restrictions that limit the value of the measurement data or do not even permit burial depth measurement at all. Therefore, there is a need for the development of a system that at least significantly reduces these limitations.

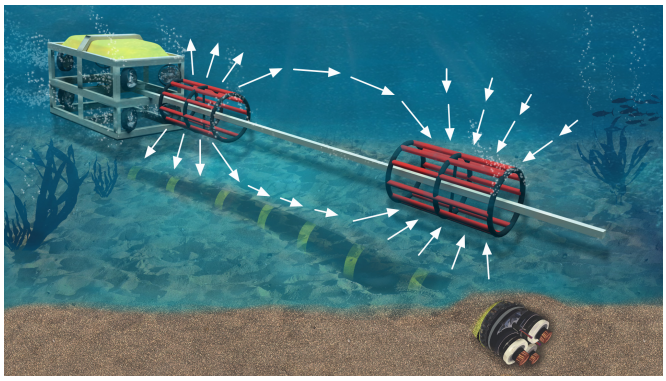

Fig. 1. Artistic rendering of EI-measuring apparatus mounted on a ROV

In order to achieve these goals and to work effectively, we estimate the expected errors of the measurements and the error propagation on the basis of an analytical model. This calculation is important for the correct inclusion of different sensors and measurements, and their weighted share in the calculation of the sensor fusion. Approaches to error propagation are rarely found, f.e. in Houston [7] and Pfaffenholz [8]. The calculations of the analytical model are verified by simulations.

II. EIT inspired platform

Electro Impedance Tomography is a non-invasive imaging technology, measuring electrical conductivity and permittivity of a spacial volume with surface electrodes. The impedance can vary considerably between different spacial regions. While some EIT systems in geophysical appliances use direct current,

978-1-7281-1450-7/19/$31.00 ©2019 IEEE

most use AC of one or several frequencies to better differentiate between materials. Typically one pair of electrodes is used to excite an electrical field in the body, while other electrodes record the resulting electrical potential. The process is repeated with different configurations of exciting and measuring electrodes. The mathematical process of recovering internal conductivities from external measurements is referred to as "Caldern's inverse problem" and allows to create a tomographic representation of the inner structure in 2D or 3D. EIT is best known for its medical applications, but is common in geophysics, material quality assurance, etc.

For our measurement system, like common practice in EIT, we measure the cable's burial depth with external electrodes, excite and measure the electric field with different electrode configurations and at multiple AC frequencies. Unlike classical EIT, we do not use the data to create a 3D or 2D image of the object in question and avoid solving the inverse problem and the tomography, because our primary interest is just one value: the cable's burial depth. Also, we skip surface electrodes but measure through the marine water.

Mounted on a remotely operated underwater vehicle (ROV), the measurement structure will move in close proximity of the seabed and align itself to the buried cable. In order to facilitate the cable's superior conductivity and oblongness, the electrode pairs are placed alongside the cables longitudinal axis. A likely form of the EI-measuring apparatus mounted on the ROV as it is currently imagined at the point of writing is given in Figure 1. The sensor part is located in front of the ROV, since it needs to operate in a environment as free of conductive material as possible. There are two sets of electrodes which allow for differential measurements to eliminate uncertainties of environmental values. This is discussed in greater detail in IV.

III. Analytical Model

As mentioned in I we aim for considerable accuracy of our measurement system. Therefore, it is crucial to be well aware of potential sources of measurement uncertainties and error margins, and it makes sense to investigate those in detail with a deductive approach. Because symbolic error propagation calculations require an analytical model to do the calculations on. Therefore, we formulate an analytical model describing the environment's electrostatic interrelations with our measurement approach. However, because models describing the real world can become arbitrarily complex and complicated, some simplifying assumptions are made so that the resulting mathematical expressions remain manageable.

- We assume the electrodes and the cables reside in one plane, which is orthogonal to the seabed. Despite that, the model extends into all three spacial dimensions and is a 3D model.
- The electrodes are metal spheres.
- Marine water and seabed are homogeneous, with the electric permittivities ε_m and ε_s.
- The seabed is smooth and parallel to both cable and electrodes.
- All thermal effects are neglected.
- The cable is an ideal conductor and modeled as two grounded metallic spheres under the electrodes in the location of the cable.
- Conductivity of seabed and water are assumed to be zero and as a result there are no electric currents.

Because some of these simplifications are significant, the validity of our results derived from this model will be discussed in respect to our assumptions in IV.

A. Deriving the Analytical Model

With the simplifications made in III, the geometry that we consider is depicted in Figure 2.

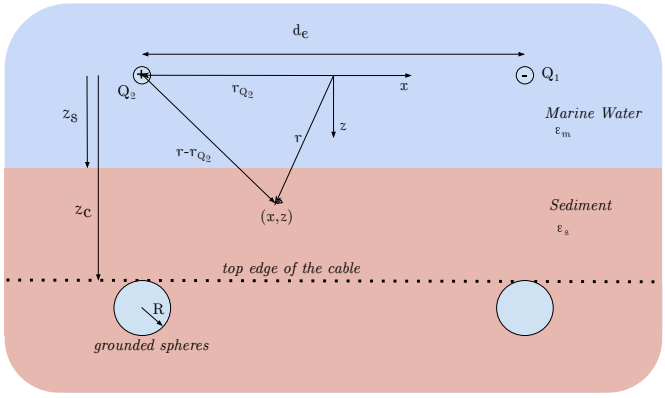

Fig. 2. Simplified geometry of electrodes, water, seabed and cable (modelled as two grounded spheres)

There is one equipotential line in this geometry: It is in the middle between the point charges and the spheres, vertical between the point charges. We utilize that when formulating the field's equation by placing the origin of the coordinate system between the point charges, aligning it's z-axis with the equipotential line. After expressing the electrical potential field of one point charge, the other one can be immediately deduced from the first by mirroring it to the other side.

Generally, the electrical potential φ at any point reached from the point charge Q by the position vector $\vec{r}$ is

$$(\varepsilon, Q, \vec{r}) \;\mapsto\; \varphi = \frac{Q}{4\,\pi\varepsilon|\vec{r} - \vec{r_Q}|}\,. \tag{1}$$

With the vector $\vec{r}$ given in our Cartesian coordinate system and expressed with x_Q and z_Q, let the first field φ_1 be

$$\varphi_1 = f\left(x - x_{Q_1}, z - z_{Q_1}, Q_1\right) \tag{2}$$

the other field φ_2 results immediately as

$$\varphi_2 = f\left(x - (-x_{Q_2}), z - z_{Q_2}, Q_2\right)\text{ , with } Q_2 = -Q_1 \tag{3}$$

and their superposition gives us the resulting scalar field

$$\varphi_{\text{res}} = \varphi_1 + \varphi_2\,. \tag{4}$$

Now, how can we assemble the electrical potential field of one point charge in our environment with the different media? Inspiration for this was received from [9]. We recognize that

one of our electrodes in water, above the sediment, is in fact a point charge in front of a dielectric half-space. This allows us to examine two cases: The first one is the electric field in water and the second one the electric field in sediment. For case one we fill the entire space with water but include only the volume above the seafloor as part of the solution. For case two we do the opposite: Fill everything with sediment and only take the seabed portion as the second half of our solution.

To express those different areas mathematically the Heaviside function $\mathcal{H}$ comes in handy. It allows piece wise definition of functions, since depending on its argument it is either zero or one. Since z_s is the distance between the origin (and the electrodes) and the seafloor, the first case, $\mathcal{H}(-z+z_s)) := \mathcal{H}_m$, is valid above the seafloor. Here $z_s - z > 0$. The second one is $\mathcal{H}(z - z_s)) := \mathcal{H}_s$, since the Heaviside's function's argument is positive for $z < z_s$.

We know that the electric field will obey the interface conditions at the boundary between water and sediment: The tangential component E_t of the electric field will be the same on both sides

$$E_{m_t} = E_{s_t}, \tag{5}$$

and the electric displacement field (with the field's normal component E_n) will be equal, too:

$$E_{m_n}\varepsilon_m = E_{s_n}\varepsilon_s. \tag{6}$$

That means we must allow for two degrees of freedom in our electric field in order to be able to satisfy these interface conditions.

For the first case of the water volume, this degree of freedom can be imagined as spreading the electric field before entering the seafloor. We introduce it by placing a mirror charge αQ at $z = -2z_s)$ below the seafloor, directly under the electrode. The resulting electric potential field in the marine water volume is caused by the electrode at a distance $x = d_e/2$ from the origin is

$$\varphi_\alpha(x,y,z) = \frac{1}{4\pi\varepsilon_0\varepsilon_m}\cdot \left(\frac{\alpha Q_1}{\sqrt{(\frac{d_e}{2}-x)^2+y^2+(-2z_s-z)^2}} + \frac{Q_1}{\sqrt{(\frac{d_e}{2}-x)^2+y^2+z^2}}\right). \tag{7}$$

For the second case which will contribute the solution for the area of the seafloor, the degree of freedom is introduced by a scaling factor β of the original charge Q_1, which gives us

$$\varphi_\beta(x,y,z) = \frac{1}{4\pi\varepsilon_0\varepsilon_m}\frac{\beta Q_1}{\sqrt{(\frac{d_e}{2}-x)^2+y^2+z^2}}. \tag{8}$$

By applying (5) and (6) to (7) and (8) we determine the factors α and β:

$$\begin{aligned}\alpha &= \frac{\varepsilon_s - \varepsilon_m}{\varepsilon_m + \varepsilon_s}\\ \beta &= \frac{2\varepsilon_m}{\varepsilon_m + \varepsilon_s}.\end{aligned} \tag{9}$$

With (9) inserted into (7) and (8) we obtain the electric potential field of one point charge in seawater above sediment given in (10).

This being the potential field caused by the first point charge, it's symmetrical twin caused by the second charge can be immediately written down with help of (3). By doing so we obtain an equation describing the resulting potential field φ_{res}, still undisturbed without a cable.

The cable's re-bar steel which protects and strengthens its structural integrity, is of course highly conductive and for the purpose of this model it is assumed to be an ideal conductor. Electric field lines always intersect perpendicularly with such ideal conductors, as do they with equipotential lines of point charges. In fact it is common practice [9] to model round (spherical) conductive objects in electric fields as equipotential surfaces of a strategically placed point charge Q_2. With s_1 being the distance between a point charge Q_1 and the center of the desired zero-potential sphere with a radius R, Q_2 needs to be placed between that sphere's center and Q_1 at a distance s_2 so that

$$\begin{aligned}R^2 &= s_1 s_2\\ \frac{Q_1^2}{Q_2^2} &= \frac{s_1}{s_2}.\end{aligned} \tag{11}$$

This simple relationship does not do justice to the underlying math, which can be found in greater detail in [9].

The placement of the point charges to model the cable is done for all other charges, in order to neutralize their effect and create a zero-potential sphere at the desired location as the cable. Thanks to the simple expression (11), this is accomplished programmatically in the case of our model. The resulting field with two electrodes, two zero-potential spheres representing the cable at a distance z_c, as well as the seabed and the marine water is thus obtained as φ_{res}.

A contour plot of the field φ_{res} with $Q = 10^{-9}C$, $d_e = 1m$, $z_s = 0.25m$, $z_c = 0.5m$, $\varepsilon_m = 76$, $\varepsilon_s = 21.75$ and the dielectric constant ε_0 results in a plausible Figure 3. The poles at the location of the point charges are blanked out for better contrast. The shapes of the potential contours bend naturally where there are no boundaries or obstructions. The transfer from seawater to sediment causes an expected visible yet steady change in the field's expansion and the point charges interact as they are supposed to.

The corresponding electric vector field is

$$\vec{E}_{\text{res}} = -\text{grad}\,(\varphi_{\text{res}}) \tag{12}$$

and is displayed with the same parameters ($Q = 10^{-9}C$, $d_e = 1m$, $z_s = 0.25m$, $z_c = 0.5m$, $\varepsilon_m = 76$, $\varepsilon_s = 21.75$) as Figure 3 in Figure 4. Exceeding long vectors around the poles

$$\varphi_1 = \frac{\mathcal{H}_m}{2\pi\varepsilon_0\varepsilon_m}\left(\frac{Q}{\sqrt{(d_e-2\,x)^2+4\,y^2+4\,z^2}}+\frac{Q(\varepsilon_m-\varepsilon_s)}{\sqrt{(d_e-2\,x)^2+4\,y^2+4\,(z-2\,z_s)^2}(\varepsilon_m+\varepsilon_s)}\right) + \frac{\mathcal{H}_s Q}{\pi\sqrt{(d_e-2\,x)^2+4\,y^2+4\,z^2}\varepsilon_0(\varepsilon_m+\varepsilon_s)} \tag{10}$$

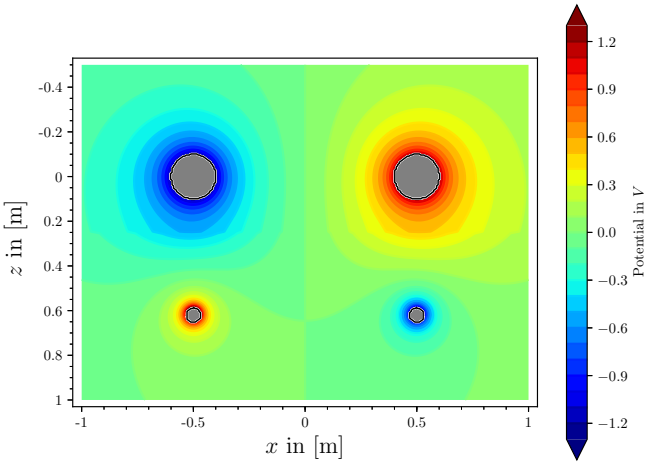

Fig. 3. Contour plot of the resulting electric potential field

are omitted for clarity. Like Figure 3, this plot serves to show the calculated field's integrity and correctness. Like in Figure 3 the transitions over the boundaries are smooth and follow the desired flow of the field. There are no unexpected changes of direction or length of the vectors, either.

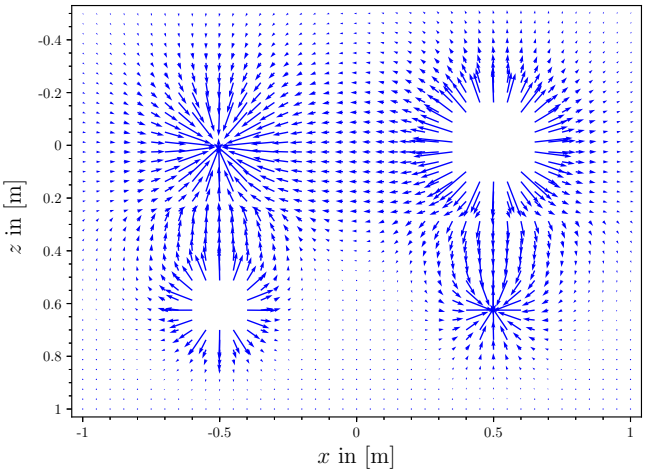

Fig. 4. Vector plot of the resulting electric field

In conclusion, the analytical model provides a specialized, simplified and plausible view into the physical interrelationships as relevant to our measurement system. But is it accurate? We will discuss that in Section III-C.

B. Applying the Analytical Model

The electric potential field's formula as given in (4) and (10) is not usable for error propagation considerations or application to real world scenarios. It contains ideal electric point charges which are unrealistic. Also, EIT operates either on voltage or current driven sources for exciting it's electrodes, not electric charges. It is possible though to calculate the required electric charge for a given configuration so that an (almost) round equipotential line in proximity of the point charge has a required electric potential (and together with the other electrode a voltage), imitating a spherical electrode.

The potential ϕ_{res} depends on (among other fixed parameters) on z_c, which changes continuously, since it is the plot's control variable. Given that we use voltage driven electrodes, their potential needs to be fixed - in our case we set it to $10V$. Being a dependant value of z_c ϕ_{res} needs to be stabilized by adjusting the charge Q for every new z_c. This is done by solving (4) for Q, as a function of z_c. This function returns the charge depending on z_c on the surface of the imaginary electrode, which is an equipotential sphere around the point charge. Inserting that equation into ϕ_{res} as the charge gives us a normed expression only depending on z_c and the fixed parameters. By multiplying it with the desired electrode voltage U we obtain the function that can be used to compare the analytical model to the simulation model by the COMSOL Multiphysics program, since it includes realistic electodes with an actual diameter, which are voltage controlled.

C. Verification against Finite Element Simulation Model

We use a 3D finite element simulation model to verify our analytical model and its prerequisites. The cable in the analytical model corresponds to an infinite conducting cylinder in 3D. Therefore we have modeled a cylinder with the cable's radius $R_{\text{cable}} = 0,3\,\text{m}$ and infinite length. The electrode is modeled as a sphere with a radius of $r_{\text{electrode}} = 0,01\,\text{m}$ and located above the cylinder. The simulation model is shown in Figure 5, where the electrode and cable are marked in color red.

The origin of z is at the boundary of seabed and seawater. The cylinder is located in the seabed at $z_c < 0\,\text{m}$ and the electrode is located in the seawater at $z_d = 0,2\,\text{m}$. The cylinder and electrode are modelled as copper elements with relative permittivity $\varepsilon_{r,\text{copper}} = 1 \cdot 10^{-15}$.

The seabed and seawater are modeled infinitely large, with a region of interest of 2m x 4m x 4m (x y z). To reduce the size of the model we took advantage of geometrical and electrical symmetries. The entire model with two electrodes of a dipole

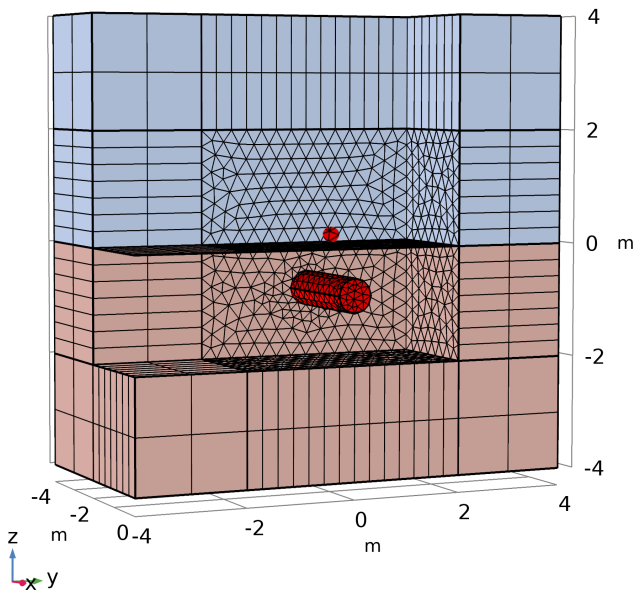

Fig. 5. COMSOL Multiphysics simulation setup, red sphere: electrode; red block: plate; blue: seawater; brown-red: seabed

is symmetrical to the YZ-plane at $x = 0\,\mathrm{m}$. We added this YZ-plane to the model and set it to ground potential. Simulations were performed on the left hand side of this plane only. Results are transformed to the right hand side by changing the sign of the values $\varphi_{\mathrm{left}}(x, y, z) = -\varphi_{\mathrm{right}}(x, y, z)$.

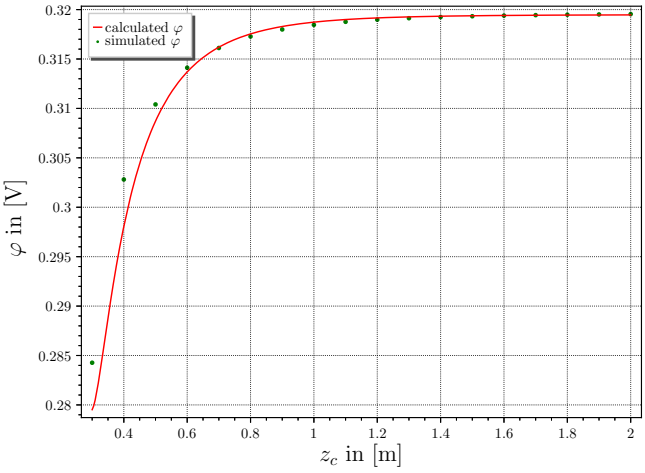

Fig. 6. Comparison of results of COMSOL Multiphysics simulation and analytical model

We performed a series of simulations by increasing the depth z_{c} in steps of $10\,\mathrm{cm}$ and thereby lowering the cable in an interval from $0.2\,\mathrm{m} - 2\,\mathrm{m}$.

Figure 6 shows the results of the electrical potential $\varphi(0.25\,\mathrm{m}, z_{\mathrm{c}})$ from simulations and the analytical model. It is a plot of the potential changed due to z_{c} increasing, at the same point between the electrodes, at x = $0.25\,\mathrm{m}$. We deduce that the simulated model with the infinite cylinder matches the results from the analytical model and validates our prerequisites for the analytical model. The results of the simulated models and the analytical model match reasonably well. Different parts of the z_{c} range highlight details of how models differ, too: At close proximity ($0.3\,\mathrm{m} < z_{\mathrm{c}} < 0.6\,\mathrm{m}$) to the cable, the spheres of the analytical model have a stronger effect than the cable in the simulation, whereas in the range ($0.6\,\mathrm{m} < z_{\mathrm{c}} < 1.2\,\mathrm{m}$), the cable's influence dominates ever so slightly. Beyond $z_{\mathrm{c}} > 1.2\,\mathrm{m}$, the difference of the two models becomes indistinguishable. We estimate that the uncertainties of parameters with highest effect on the models will have the highest effect on real applications also.

Now that we verified the validity of the analytical model against the simulation in COMSOL Multiphysics, we go ahead and use it to calculate the intervals of uncertainties of our parameters.

IV. Evaluation of Critical Environmental Parameters

For scientific measurements it is a standard procedure to consider the propagation of errors as an effect of variables' uncertainties, or random errors (in contrast to systematic errors) as described in [10]. Every measurement is subject to uncertainties due to measurement limitations which propagate due to the processing of this input to functions and algorithms.

For calculating and visualizing the error intervals and boundaries we use the computer algebra system Sage [11] with features covering most aspects of mathematics, including statistics and specifically error propagation. For that, it uses MPFI (Multiple Precision Floating-Point Interval Library), based on MPFR (Multiple-Precision Floating-point computations with correct Rounding). That library is well suited for identifying the most severe sources of uncertainty in our measuring system and calculating the guaranteed result interval of the cable's burial depth.

A. Analytical Model Parameters' Intervals of Uncertainty

Our analytical model has seven input parameters and their values are subject to measurement uncertainties:

- the distance between the centers of the electrodes d_e,
- the distance between the centers of the electrodes and the sediment z_s,
- the distance between the centers of the electrodes and the top edge of the cable z_c,
- the electrical permittivity of marine water ε_m,
- the electrical permittivity of the sediment ε_s,
- the exciting voltage U (caused by the charge Q) and
- the measured potential difference ΔU.

Of these measurements , the cable depth z_c is the resulting value we want to determine.

The values that depend on our own measurement system are still estimates, as we do not have a working prototype yet. Especially one, the expected working distance to the sea floor z_s, is hard to specify with a good degree of accuracy, since we want to measure with ROVs that fly over the seabed. That parameter's accuracy is complicated further by the fact that

TABLE I
PARAMETERS AND THEIR INTERVAL VALUES

Parameter	**value interval**	**source/reference**
d_e	0.999-1.001m	estimated
z_s	0.2-0.3m	estimated
z_c	to be determined	calculated
ε_m	75-77	[12]
ε_s	3.5-40	[13]
U	9.99-10.01V	estimated
ΔU	$\pm 0.01V$	estimated

the transition from marine water to sediment is not an abrupt but rather a gradual one, with the water content of the ground decreasing downwards. Also, the surface of the seafloor often features ripples of varying sizes, causing distortions and hot spots in the electric flow. These ripples also cause ambiguities when determining distance, especially since the electric flow fans out in the water, making the effective area on the seafloor bigger then one such ripple. The electric permittivity of sea water and seafloor are taken from [12] and [13], respectively.

Now we have all required prerequisites to calculate and plot the electrical potential interval of any point in our geometry, depending on our input parameters and their value's interval. Because the injecting electrodes are part of the measuring system, we select a point with the same z_c as the electrodes, at $(x, z) = (0.25m, -z_c)$.

The resulting plots are aggregated in Figure 7. The left column displays the interval of uncertainty if just that value had an uncertainty. The right column shows the system's remaining measurement uncertainty if that one value was perfectly known. In the next chapter we will examine these plots and learn as much from them as possible.

B. Discussing the Results of the Plots

All the plots in the right column of Figure 7 feature an uncertainty interval dominating the value range. For the entire range of mappings $z_c \mapsto \varphi$ there are mappings to equally large parts of the vertical φ axis. That means that unambiguous measurements would be hard to obtain without further remedial actions. That is a detrimental feature for any measurement system. A positive aspect is, that the errors are entirely independent of cable depth. Increased burial depth does not result in additional or widening error margins.

By comparing the residual error margins in the right column, it becomes easy to identify the dominant error source, which is the sediment's electrical permittivity. Given that ε_s's relative error is 83% that does not surprise. ε_s is also the parameter that is hardest to determine. Only the surface of the seabed is directly accessible, and does not tell a lot about deeper layers. In the North Sea and Baltic Sea it is quite common for the seabed to change substantially on the first meter downwards and its layers to alter significantly over a distance of 10m. So our measuring system will need to adapt to this challenge. The impulse neutron sensor that we will use in our sensor fusion will hopefully provide useful data to reduce this factor. The

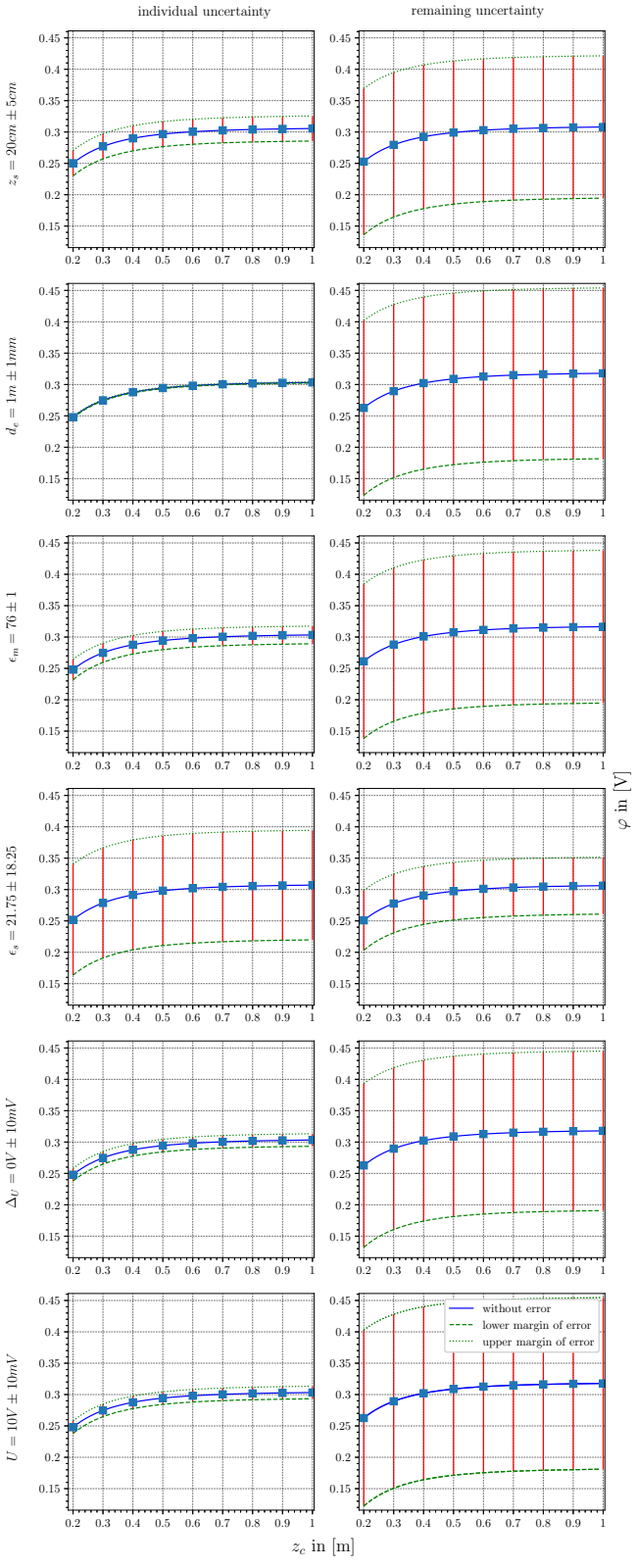

Fig. 7. Comparison of uncertainties of values and their effects on the measurement of cable depth.

thermal changes introduced by the losses of the cable will play an important role here, too.

The influence of the distance to the seafloor z_s's uncertainty is the second biggest individual margin of error. The corresponding graph in the right column shows a noticeable improvement compared to the worst case graph right below. The altimeter will give us additional data regarding the distance to the seafloor and its surface structure, but the seafloor's ripple effect and the gradual shift from sea water to seafloor remain an unknown issue until we can conduct real world experiments.

An uncertainty that might be easy to reduce is the one of ε_m. Its effect is less then z_s's and greater than ΔU's and U's. The remaining margin of error depicted on the right hand side is consequently still very significant. None the less, an additional permittivity sensor for determining ε_m could let us drop this value from search algorithms and provide additional stability to e.g. a gradient descent method.

The least critical value according to this chart is d_e. It contributes hardy any uncertainty to the end result. It remains to be seen whether or not the measurement apparatus can be constructed in a way that mechanical bending and thermal expansion and shrinkage remain within the margin of $\pm 1mm$.

The parameters ΔU and U contribute a very similar individual effect to the overall measurement uncertainty. Their margins of error are also comparatively easy to control and reduce by more sophisticated hardware. While they must not be neglected, they are certainly not the highest priority to improve, given their small influence on the overall error of the system.

In conclusion of this discussion, the largest contribution to the overall margin of error is the composition of the seafloor. It dwarves the remaining investigated sources of uncertainty combined. Hopefully both the sub bottom profiler and the impulse neutron sensor can help here. Independently from their input, we plan a differential measurement approach. In the exact same $x - y$ spot of the seabed we will conduct the same impedance measurement at different vertical distances z_s from the seabed with well known Δz_s between our sets of measurement electrodes. This differential measurement will help to reduce both ε_s and z_s errors as well as other uncertainties.

In III we mentioned that the simplifications we made needed to be considered when discussing results of this paper. From 6 we see that the characteristic curve of the match well and we assume that it's description of reality with its limited scope is accurate. Therefore we have reason to believe that our analysis of measurement uncertainties is correct as well. The limitations of the model by excluding thermal effect and conductivity remain. Those parameters will contribute additional uncertainties, but the identified ones and their interrelations will not change fundamentally. The results presented in this paper remain a valuable and important contribution as we identify critical parameters for our measurement system.

V. Conclusion and Outlook

In this paper we introduce a yet unsolved problem of measuring the depth of an undersea cable with a required accuracy of $\pm 10\ cm$ in a typical depth of $1\ m$. We developed an analytical model for calculating the potential based on an electrical static field for this problem. We evaluated and validated the model by simulations with COMSOL Multiphysics. The advantage of this model is that it identifies and evaluate the critical parameters in the measurement setup. The main critical parameter is identified as the permittivity of the subsea sediment ε_s. This result will help us to identify crucial risks for our measurement system and we will consider them in the process of the project. For the future, we will implement an electrical impedance tomography (EIT) measurement system with multiple frequencies for localization of cables in the seabed. To address the results of our analytical results, we will integrate sensor fusion, with an optical control unit, a sub-bottom profiler and a pulse neutron sensor with the EIT platform to measure and consider the critical parameters in the measurement system. The analytical model will be extended by conductivity in the future.

VI. Acknowledgements

This is a joint effort of Sea & Sun Technology GmbH, J&C Bachmann GmbH, Technische Hochschule Lübeck and Fugro Germany Marine GmbH, which is funded by the Federal Ministry of Economic Affairs and Energy of the Federal Republic of Germany (project number: 03SX467B). Horst Hellbrück is adjunct professor at the Institute of Telematics of University of Lübeck.

References

[1] Tinsley. (2019) Submarine cable survey & tracking system model 5930 mk ii. [Online]. Available: http://tinsley.co.uk/wp/?page_id=1785

[2] S. Cowls and S. Jordan, "The enhancement and verification of a pulse induction based buried pipe and cable survey system," in *OCEANS'02 MTS/IEEE*, vol. 1. IEEE, 2002, pp. 508–511.

[3] T. Szyrowski, S. K. Sharma, R. Sutton, and G. A. Kennedy, "Developments in subsea power and telecommunication cables detection: Part 2-electromagnetic detection." *Underwater Technology*, vol. 31, no. 3, 2013.

[4] P. Church, J. E. McFee, S. Gagnon, and P. Wort, "Electrical impedance tomographic imaging of buried landmines," *IEEE Transactions on Geoscience and Remote Sensing*, vol. 44, no. 9, pp. 2407–2420, 2006.

[5] G. Bouchette, P. Church, J. E. Mcfee, and A. Adler, "Imaging of compact objects buried in underwater sediments using electrical impedance tomography," *IEEE Transactions on Geoscience and Remote Sensing*, vol. 52, no. 2, pp. 1407–1417, 2014.

[6] C. Xu, J. Chen, D. Yan, and J. Ji, "Review of underwater cable shape detection," *Journal of Atmospheric and Oceanic Technology*, vol. 33, no. 3, pp. 597–606, 2016.

[7] M. H. Houston, "Cable positioning using compasses, tailbuoys, and acoustic devices," in *SEG Technical Program Expanded Abstracts 1991*. Society of Exploration Geophysicists, 1991, pp. 761–763.

[8] J. Paffenholz, D. Monk, and D. Fryar, "Random and systematic navigation errors: How do they affect seismic data quality?" *First Break*, vol. 12, no. 10, pp. 505–513, 1994.

[9] vanRienen. (2018) Vorlesungsscript Theoretische Elektrotechnik. [Online]. Available: https://www.iae.uni-rostock.de/fileadmin/uni-rostock/Alle_IEF/IAE/Lehre/ThET/ThET_Skript.pdf

[10] Beuth-Verlag, "DIN 1319-2, Messtechnik, Grundlagen der Messtechnik."

[11] W. A. Stein. Sage math. [Online]. Available: https://www.sagemath.org

[12] T. Meissner and F. J. Wentz, "The complex dielectric constant of pure and sea water from microwave satellite observations," *IEEE Transactions on Geoscience and remote Sensing*, vol. 42, no. 9, pp. 1836–1849, 2004.

[13] A. Martinez and A. P. Brynes, *Modeling dielectric-constant values of geologic materials: An aid to ground-penetrating radar data collection and interpretation*. Kansas Geological Survey Lawrence, Kansas, 2001, vol. 247.